



## Synthesis and Characterization of ZnO-Ag Nanoparticles Supported on MCM-41 as Photocatalyst

EVA M. BARRERA-RENDÓN<sup>1,2</sup>, JAIME JIMÉNEZ-BECERRIL<sup>2\*</sup> and GENOVEVA GARCÍA-ROSALES<sup>1</sup>

<sup>1</sup>Departamento de Estudios de Posgrado e Investigación, Instituto Tecnológico de Toluca, Metepec, México.

<sup>2</sup>Departamento de Química, Instituto Nacional de Investigaciones Nucleares, Cd. De México, México.

\*Corresponding author E-mail: jaime.jimenez@inin.gob.mx

<http://dx.doi.org/10.13005/ojc/330212>

(Received: October 13, 2016; Accepted: February 02, 2017)

### ABSTRACT

Development of photocatalyst is a key step for separation of photocatalyst to solution supported materials. ZnO-Ag/MCM-41 nanoparticles synthesized by a wet process were studied as photocatalysts in the Congo red photodegradation, which is a water contaminant. Also were used prepared zinc oxide, commercial zinc oxide, silver doped zinc oxide, Mobil Catalytic Material No. 41, zinc oxide supported on MCM-41, and commercial zinc oxide supported on MCM-41. All systems were characterized by SEM, FTIR, XRD, and surface area by BET and tested in photocatalytic degradation of Congo red. It was found that the systems showed the crystalline phase wurtzite for ZnO, and a main amorphous component for MCM-41, ZnO/MCM-41 and ZnOC/MCM-41. The materials had different particle size and morphology; however, predominantly spherical nanoparticles (less than 100 nm) were found. For photocatalytic UV irradiation a maximum degradation of 30% for 120 min was reached with a ZnO-Ag as catalyst.

**Keywords:** Nanoparticles; Photodegradation; Congo red; ZnO supported

### INTRODUCTION

In textile industry, dyes are used as raw material, which generates 525,000 tons per month of waste water<sup>1</sup>; as example of dye used in the past is the Congo red, which was prohibited because of its toxicity, mutagenic and carcinogenic properties. Some alternative solutions to eliminate

such pollutants are studied<sup>2</sup>. By nanotechnology synthesis it is possible to obtain new materials with specific properties, among them the photocatalytic activity is a viable option for the degradation of organic pollutants<sup>3</sup>. Photocatalysis belongs to AOP (Advanced Oxidation Processes) for destruction of chemical pollutants where hydroxyl radicals are produced to oxidize organic compounds.

Photocatalysis is the activation of a photochemical reaction using ultraviolet light or visible light as chemical energy by the presence of a catalyst substrate<sup>4</sup>. Zinc oxide (ZnO) is a photocatalyst reported in the literature, it has photocatalytic activity, strong oxidative capacity, and lower cost, which make it attractive solution for waste water treatment<sup>5</sup>. Besides, it has an open hexagonal close packed lattice where Zn atoms occupy half of the tetrahedral sites while all the octahedral sites are empty. Hence, there are sites available accommodating higher doping concentration limits in the host lattice<sup>6</sup>. The presence of Ag improves its photocatalytic properties<sup>7,8</sup>, by promoting interfacial electron-hole spacing<sup>9</sup> and the Ag addition may trap photogenerated electrons<sup>10</sup>.

In studies with silver doped zinc oxide (ZnO-Ag) nanoparticles, if the photocatalyst is synthesized in nanosize scale, its manipulation becomes difficult for the treatment of effluents<sup>11</sup>, and there are not experiments using Mobil Catalytic Material No. 41 (MCM-41) as support, however, it does with others. Lu<sup>12</sup> prepared chitosan-Ag/ZnO composite, and they found that supporting photocatalyst is an effective way to reduce the amount of nanoparticles; The use of only ZnO/Ag nanoparticles has the disadvantage of release nanoparticles into the environment during the treatment process poses a health risk, so, nanoparticles typically must be supported on substrates such as clays such as bentonite<sup>13</sup>.

In this research is focused to support ZnO-Ag, for that, nanoparticles of ZnO-Ag/MCM-41, ZnO, commercial zinc oxide (ZnOC), ZnO-Ag, MCM-41, ZnO/MCM-41, ZnOC/MCM-41 were synthesized by wet method and were characterized and evaluated their photodegradation activity of Congo Red.

## Method

### Materials

Sigma Aldrich reagents of dihydrate zinc acetate, AgNO<sub>3</sub>, hydrogen peroxide 30%, hexadecyltri-methylammonium bromide, ethylamine, tetra-methylammonium hydroxide, and tetraethylorthosilicate were used for synthesis.

### Synthesis of ZnO nanoparticles

For synthesis of ZnO nanoparticles, were prepared 1.087 g of dihydrate zinc acetate on 150

mL of distilled water. Mixture of 15 mL of hydrogen peroxide 30% was added with constant agitation, and maintained at reflux for 2 hour. Particles formed were recovered by centrifugation at 6000 rpm and dried at 80°C. Then the material was heat treated at 300°C for 2 hours.

### Synthesis of ZnO-Ag nanoparticles

To obtain ZnO-Ag nanoparticles, 1.3 g of AgNO<sub>3</sub> on 7.5 mL of distilled water in constant agitation was added the ZnO nanoparticles during 1 h. Then, they were dried at 80°C of temperature for 6 h. ZnO-Ag nanoparticles were heat treated at 300°C for 2 hours.

### Synthesis of MCM-41

For the preparation of MCM-41 was used the method reported by Yin<sup>14</sup>. 2.43 g of hexadecyltrimethylammonium bromide was dissolved in 67 mL of water. A solution of 1.11 mL of ethylamine and 6 mL of tetramethylammonium hydroxide was added. Then 8 mL tetraethylorthosilicate was added. The solution was aged for 24 hours. Particles formed were recovered by centrifugation at 5000 rpm and then dried at 80°C for 24 hours. Finally, the material was calcined for 5 h at 550°C.

### Synthesis of ZnO-Ag/MCM-41

For obtain the material of ZnO-Ag/MCM-41, in 5 mL of distilled water were suspended 0.04 g of ZnO-Ag nanoparticles, 3 g of MCM-41 were added with agitation during 1 hour.

For ZnO/MCM-41 and ZnOC/MCM-41 systems, syntheses were conducted like in ZnO-Ag/MCM-41 synthesis.

### Sample characterization

The morphology was examined using a scanning electron microscope (SEM, JEOL JSM-6610LV). The structural and phase identification of samples were characterized by a powder X-ray diffraction (XRD, Bruker D8 Discover). The functional groups identification of samples was characterized by IR spectrometer with Fourier transform (FTIR, Magna-IR Spectrometer 550). The absorbance of Congo red solution was measured by a UV-Vis spectrophotometer (UV-Vis Lambda 25 Perkin Elmer).

### Photocatalytic activity test

Congo red (CR) dye was used as a dye model to evaluate a photocatalytic degradation of samples response to UV irradiation at room temperature. The experiments were carried out as follows: 100 mg of sample were dispersed into 100 mL of a 20 mg/L CR solution in a glass beaker. Prior to irradiation, the mixtures were stirred in the dark for 1 hour to ensure equilibrium of CR adsorption and desorption, then the samples had an irradiation with an UV lamp (black light at  $\lambda = 354$  nm, 8 W), at a distance of 10 cm from a glass beaker. At given intervals (1 h), 5 mL samples of the mixtures were collected and subsequently filtered to separate solid and solution. Then, remained CR was determined at 497 nm in a Perkin Elmer, Lambda 35 UV/Vis spectrophotometer.

### RESULTS and DISCUSSIONS

#### Morphological study

In this study, SEM was used to characterize a particle shape of ZnO-Ag/MCM-41, ZnO, ZnOC, ZnO-Ag, MCM-41, ZnO/MCM-41, ZnOC/MCM-41 particles and the electron images are presented in Fig. 1. The particle shape of ZnO powder (Fig. 1b) changed from different size and morphology to define agglomerated nanoparticle shape when loading with Ag (Fig. 1d) and MCM-41 (Fig. 1e). This might be due to the different surface properties that had been influenced by Ag and MCM-41 and then affected the different growth mechanisms of pure ZnO and the ZnO-Ag, ZnO/MCM-41 (Fig. 1f), ZnOC/MCM-41 (Fig. 1g), ZnO-Ag/MCM-41 (Fig. 1a) systems. It was of interest, that a hexagonal ZnO

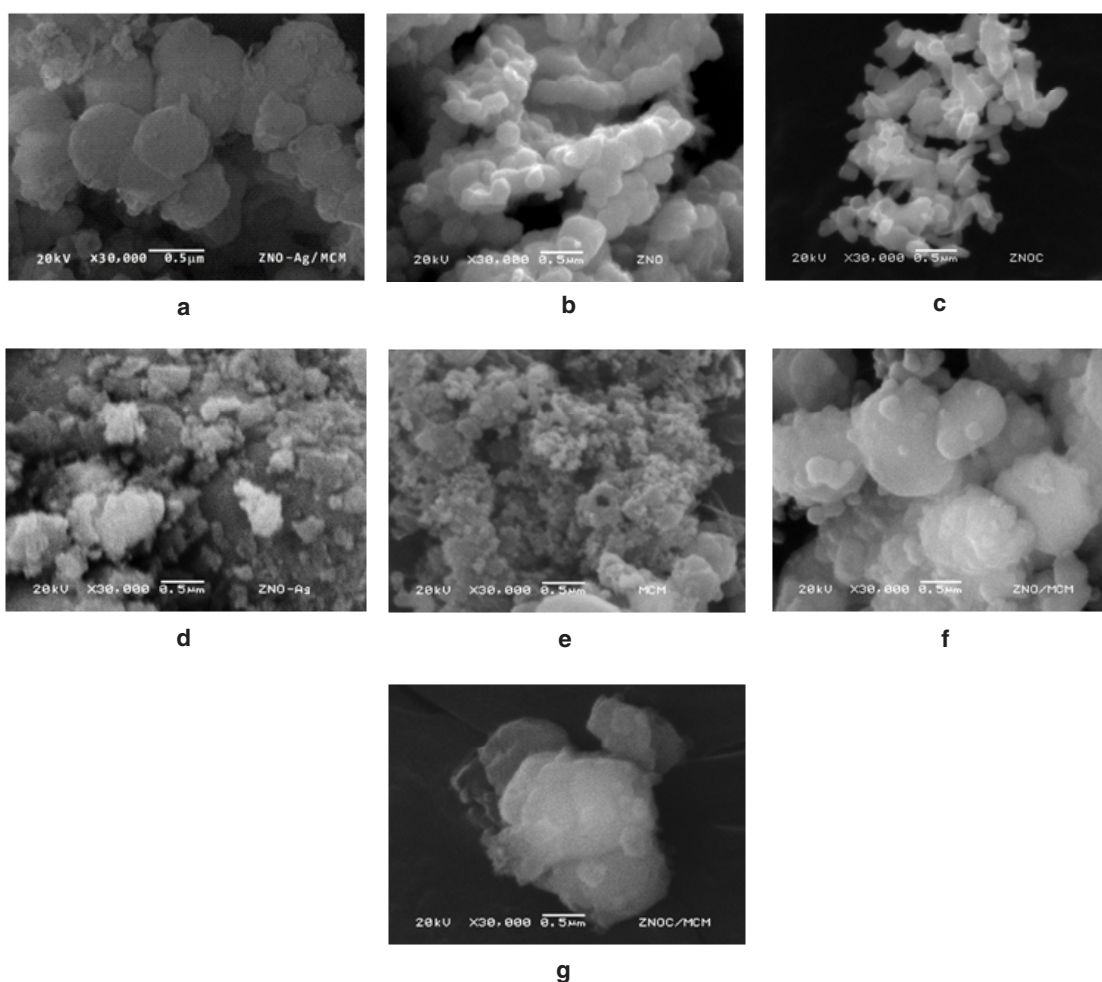


Fig. 1: SEM of a) ZnO-Ag/MCM-41, b) ZnO, c) ZnOC, d) ZnO-Ag, e) MCM-41, f) ZnO/MCM-41, g) ZnOC/MCM-41

grew independently when loaded with Ag, this might be due to a larger particle size having a lower surface energy, so an agglomeration of particles that would

reduce a surface energy did not occur<sup>15</sup>. The MCM-41 particles are spheres with different sizes and when loading with ZnO, ZnOC (Fig. 1c) and ZnO-Ag it

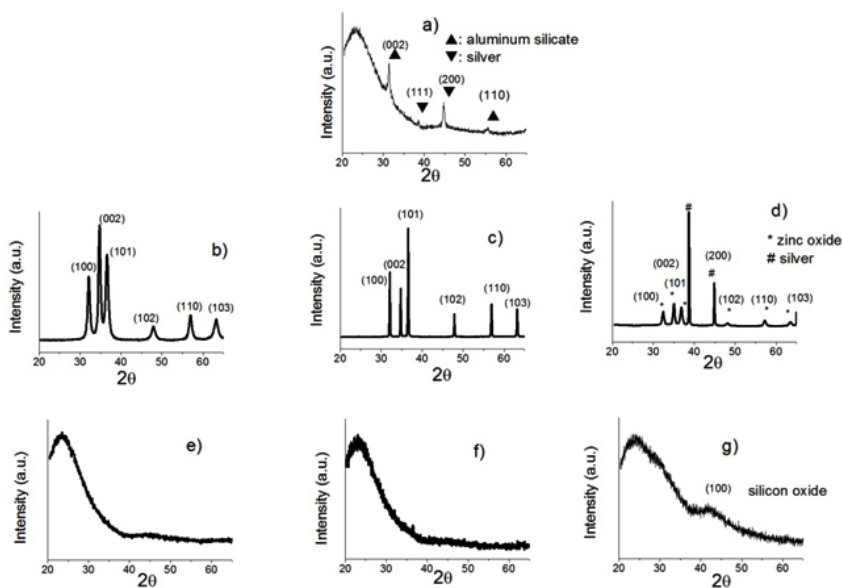


Fig. 2: XRD of a) ZnO-Ag/MCM-41, b) ZnO, c) ZnOC, d) ZnO-Ag, e) MCM-41, f) ZnO/MCM-41, g) ZnOC/MCM-41

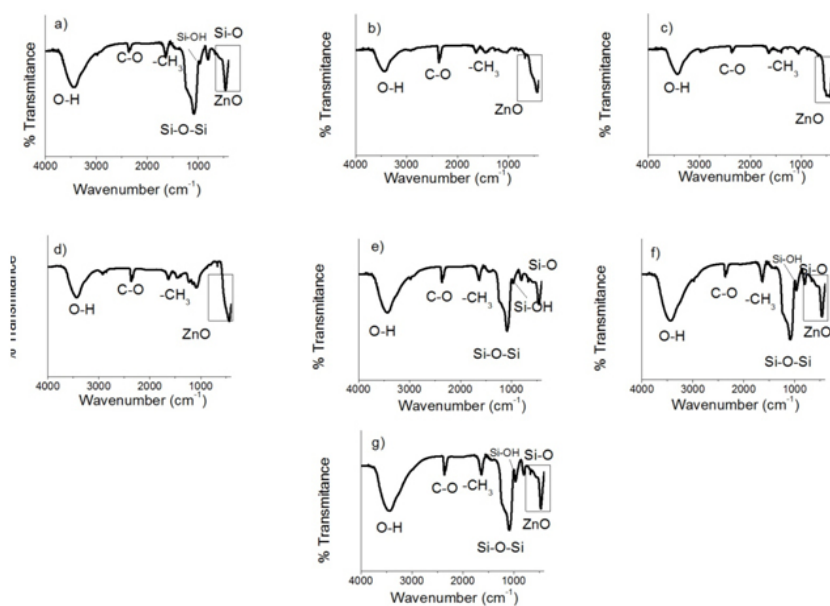


Fig. 3: FT-IR of a) ZnO-Ag/MCM-41, b) ZnO, c) ZnOC, d) ZnO-Ag, e) MCM-41, f) ZnO/MCM-41, g) ZnOC/MCM-41

observed that the size higher than without loading and the morphology are much defined (Table 1). In other hand, elemental analysis results showed the elements in each system (Zn, O, Ag, Si, Al, C).

### Phase identification

The XRD patterns of ZnO-Ag/MCM-41, ZnO, ZnOC, ZnO-Ag, MCM-41, ZnO/MCM-41, ZnOC/MCM-41 particles are presented in Fig. 2. For ZnO-Ag/MCM-41, Fig. 2a) shows presence of aluminum silicate (JCPDS No. 00-052-0142), and metallic Ag (JCPDS No. 00-004-0783). Also it is observed presence of amorphous material due to MCM-41. For ZnO Fig. 2b) and ZnO commercial Fig. 2c), the main patterns are hexagonal wurtzite (JCPDS No. 00-036-1461); the different intensities prove the small size of the particles. The XRD patterns in Fig. 2d) also exhibited a small peak

of metallic Ag at 38.8 and 44.9  $2\theta$  in its cubic and wurtzite phase; this indicate that ZnO-Ag nanoparticles were completely formed<sup>16, 17</sup>. Fig. 2e, 2f and 2g) show amorphous material of silicon oxide, component of MCM-41, besides the difference between ZnO/MCM-41 and ZnOC/MCM-41 is the silicon oxide peak in 42.41  $2\theta$ , caused for ZnOC.

### IR characterization

In Fig. 3 are presented the FT-IR spectra of the ZnO-Ag/MCM-41, ZnO, ZnOC, ZnO-Ag, MCM-41, ZnO/MCM-41, ZnOC/MCM-41. The main infrared absorption peaks are located in the middle and lower frequency zones. Hydroxyl groups and water molecules are confirmed by the broad bands detected at high frequency at around 3432  $\text{cm}^{-1}$ , where the broadening of this band is due to O-H bond. The peak at 1612  $\text{cm}^{-1}$  belongs to  $-\text{CH}_3$  vibrations from the surfactant of zinc acetate and it becomes remarkable after thermal treatment<sup>18</sup>. The band from 1260 to 1006  $\text{cm}^{-1}$  represents Si-O-Si functional group; the peaks in 988  $\text{cm}^{-1}$  and 760 belong to Si-OH and Si-O vibrations from the mesoporous MCM-41<sup>19</sup>. IR spectra of ZnO show that absorption peaks in the range 600-400  $\text{cm}^{-1}$ , indicating the formation of ZnO nanospheres assembled microspheres<sup>18, 20, 21</sup>.

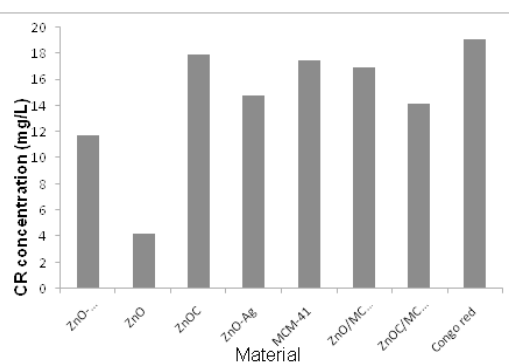


**Fig. 4: Adsorption of CR at [20 mg/L] with irradiation time for 0 min**

### Surface area analysis

BET surface area analysis has been done by  $\text{N}_2$  physical adsorption on the particle surface and the obtained data were summarized in the Table 1. The largest surface area is presented for sample

**Table 1: Elemental analysis EDX of ZnO, ZnOC, ZnO-Ag, MCM-41, ZnO/MCM-41, ZnOC/MCM-41 and ZnO-Ag/MCM-41**

Material	Size (nm)	Surface area( $\text{m}^2\text{g}^{-1}$ )	Zn	O	% Ag	% atomic Si	Al	C
ZnO	64	8.6	40.6	59.4	-	-	-	-
ZnOC	141	5.2	52.7	47.3	-	-	-	-
ZnO-Ag	67	5.1	34.3	59.0	6.7	-	-	-
MCM-41	33	1120.0	-	23.5	-	18.5	27.8	30.2
ZnO/MCM-41	122	1030.0	0.1	62.6	-	17.9	-	19.4
ZnOC/MCM-41	38	1090.0	0.1	65.2	-	14.4	-	20.3
ZnO-Ag/MCM-41	202	1040.0	0.1	70.6	0.3	28.8	0.2	-

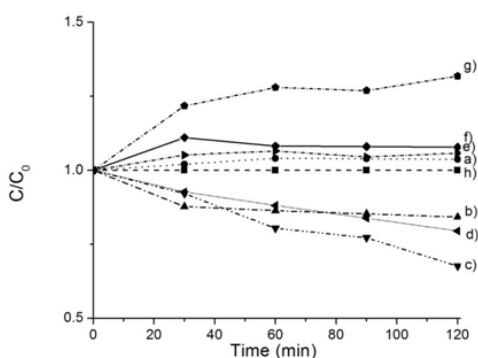


**Fig. 5: Photocatalysis test of CR degradation at [20 mg/L] with irradiation time for 120 min of: a) ZnO-Ag/MCM-41, b) ZnO, c) ZnOC, d) ZnO-Ag, e) MCM-41, f) ZnO/MCM-41, g) ZnOC/MCM-41 as catalysts and h) without catalyst**

MCM-41 ( $1120 \text{ m}^2\cdot\text{g}^{-1}$ ), similar to López<sup>22</sup>, and the smallest surface area belongs to ZnO-Ag ( $5.1 \text{ m}^2\cdot\text{g}^{-1}$ ). This fact confirms that the metal presence has influence on the surface area, which was closely related to the catalytic activity<sup>23</sup>. Specifically, the silver presence implied a smaller surface area, which could be caused from the formation of larger ZnO crystals with high crystallinity<sup>24, 25</sup>.

#### Photocatalytic activity

Fig. 4 shows the adsorption of CR in used materials; the results indicate that ZnO is the material which possess a bigger adsorption than ZnO-Ag/MCM-41, this result coincide with the surface area ( $8.6$  and  $1040 \text{ m}^2\cdot\text{g}^{-1}$ , respectively); if the area is smaller, the contact area with the pollutant is bigger. ZnOC has the smaller adsorption of all materials, this is because it is not a nanoparticle ( $141 \text{ nm}$ ) and it does not have spherical form.

The photocatalysis of ZnO-Ag/MCM-41, ZnO, ZnOC, ZnO-Ag, MCM-41, ZnO/MCM-41, ZnOC/MCM-41 was assessed by the photodegradation of CR with UV light irradiation. Fig. 5 shows the CR removal efficiency as a function of irradiation time using different solid catalysts. The blank test without catalysts testified that the photoinduced self-decomposition of CR was negligible.

The degradation efficiency of single component ZnO sample was only 16% with 2 hours

of irradiation like in the Fig. 5b). In the Fig. 5d) the as prepared ZnO/Ag improves photocatalytic activity at 20% of CR remotion from the solution after 2 hours irradiation. The enhanced photocatalytic activity of the ZnO-Ag particles can be interpreted firstly, the coupling of silver with ZnO supports created numerous high-specific-surface interphase boundaries that had an important influence on their physical properties<sup>26</sup>. Besides, the synthesis of ZnO-Ag induced the strong electronic coupling between ZnO and Ag, inhibiting the photogenerated electron-hole recombination and greatly prolonging the life time of charge carriers<sup>10</sup>. In other hand, the mesoporous MCM-41 in Fig. 5e), only adsorbs the CR and when is loaded with ZnO, ZnOC and ZnO-Ag (Fig. 5a, 5f, 5g), desorbs from 3% to 30%.

The observed photodesorption in MCM-41, ZnO/MCM-41 and ZnOC/MCM-41 materials is because there are some phenomena on the surface of materials. The photodesorption occurred during light irradiation the adsorbed oxygen on ZnO is pumped away from the surface and oxygen from the ambient environment is re-adsorbed; the presence of carbon favors chemisorption of oxygen onto the surface and an electron is capture from the conduction band to form  $\text{CO}_2^-$ ; the ion may be neutralized by photohole under UV illumination<sup>27</sup>. Then, conductivity and photocatalytic efficiency decrease.

#### CONCLUSIONS

It was successfully prepared ZnO-Ag nanoparticles supported on MCM-41 synthesized wet process. The main morphology of samples is spherical. The synthesized ZnO-Ag material exhibited excellent CR photocatalytic degradation after UV irradiation for 120 minutes, which could be a promising photocatalyst in removing organic pollutants from waste water. The ZnO-Ag/MCM-41 material has a desorption behavior, caused by surface phenomena, mainly oxygen adsorption-desorption during UV irradiation.

#### ACKNOWLEDGEMENT

The authors thank to CONACYT for scholarship No. 663749, to ININ (project No. CB-504) and Instituto Tecnológico de Toluca for support (project No. DGEST 5894.16-P).

## REFERENCES

- 1 INEGI (Instituto Nacional de Estadística Geográfica e Informática)**2003**, Available at: <http://www3.inegi.org.mx/sistemas/biblioteca/ficha.aspx?upc=702825000039> Accessed on 26 March **2015**.
- 2 Dafare, S.; Deshpande, P.S.; Bhavsar, R.S. *Indian J. Chem. Techn.***2013**, *20*, 406-410
- 3 Shemer, H.; Sharpless, C.M.; Linden, K.G. *Water Air Soil Poll.***2005**, *168*, 145-155
- 4 Ohama, Y.; Van Gemert, D. Application of titanium dioxide photocatalysis to construction materials, 1st edn. *Springer, USA*, **2011**, *1*.
- 5 Saoud, K.; Alsoubaihi, R.; Bensalah, N.; Bora, T.; Bertino, M.; Dutta, J. *Mater. Res. Bull.***2015**, *63*, 134-140
- 6 Sahu, R.K.; Ganguly, K.; Mishra, T.; Mishra, M.; Ningthoujam, R.S.; Roy, S.K.; Pathak, L.C.; *J. Colloid Interf. Sci.***2012**, *366*, 8-15
- 7 Zhao, Z.; Wang, M.; Liu, T. *Mater. Lett.***2015**, *158*, 274-277
- 8 Chen, P.; Gu, L.; Xue, X.; Song, Y.; Zhu, L.; Cao, X. *Mater. Chem. Phys.***2010**, *122*, 41-48
- 9 Bechambi, O.; Chalbi, M.; Najjar, W.; Sayad, S. *Appl. Surf. Sci.***2015**, *347*, 414-420
- 10 Xie, W.; Li, Y.; Sun, W.; Huang, J.; Xie, H.; Zhao, X. *J. Photoch. Photobio A.***2010**, *216*, 149-155
- 11 Huang, H.; Wang, H.P.; Chang, J.; Wei, Y. *J. Electron Spectrosc.***2007**, *156-158*, 357-360
- 12 Lu, Z.; Gao, J.; He, Q.; Wu, J.; Liang, D.; Yang, H.; Chen, R. *Carbohydr. Polym.***2016**, doi:10.1016/j.carbpol.2016.09.051
- 13 Motshega, S.C.; Ray, S.S.; Onyango, M.S.; Momba, M.N.B. *Appl. Clay. Sci.***2015**, *114*, 330-339
- 14 Yin, A.; Wen, C.; Dai, W.; Kangnian, F. *Appl. Catal. B-Environ.***2011**, *108-109*, 90-99
- 15 Klubnuan, S.; Amornpitoksuk, P.; Suwanboon, S. *Mat. Sci. Semicon. Proc.***2015**, *39*, 515-520
- 16 Wang, L.; Hou, X.; Li, F.; He, G.; Li, L. *Mater. Lett.***2015**, *161*, 368-371
- 17 Hou, X. *Mater. Lett.***2015**, *139*, 201-204
- 18 Reddy, M.M.; Reddy, G.R.; Chennakesavulu, K.; Sundaravadivel, E.; Prasath, S.S.; Rabel, A.M.; Sreeramulu, J. *J. Porous Mater.***2016**, doi:10.1007/s10934-016-0247-3
- 19 Kiomarsipour, N.; Razavi, R.S.; Ghani, K. *Dyes Pigments.***2013**, *96*, 403-406
- 20 Wang, Y.; Zhou, G.; Guo, J.; Liu, T. *Ceram. Int.***2016**, *42*, 2467-2474
- 21 Bera, S.; Khan, H.; Biswas, I.; Jana, S. *Appl. Surf. Sci.***2016**, *383*, 165-176
- 22 López, L. P.; Van Eck, E.R.H.; Melián-Cabrera, I. *Micropor. Mesopor. Mat.***2016**, *220*, 88-98
- 23 Li, D.; Haneda, H. *Chemosphere.***2003**, *51*, 129-137
- 24 Yu, C.; Yang, K.; Xie, Y.; Fan, Q.; Yu, J.C.; Shu, Q. *Nanoscale.***2013**, *5*, 2142-2151
- 25 Muñoz-Fernandez, L.; Sierra-Fernandez, A.; Milošević, O.; Rabanal, M.E. *Adv. Powder Technol.***2016**, *27*, 983-993
- 26 Tietze, T.; Audehm, P.; Chen, Y.C.; Schütz, G.; Straumal, B.B.; Protasova, S.G. *Sci. Rep.***2015**, *5*, 8871
- 27 Zhang, D.H. *Mater. Chem. Phys.***1996**, *45*, 248-252